Arabian Journal of Chemistry (2022) **15**, 103636

King Saud University

Arabian Journal of Chemistry

www.ksu.edu.sa
www.sciencedirect.com

ORIGINAL ARTICLE

Corrosion product formation on zinc-coated steel in wet supercritical carbon dioxide

Ville Saarimaa [a,*], Aaretti Kaleva [b], Arnold Ismailov [b], Tero Laihinen [a], Markus Virtanen [a], Erkki Levänen [b], Pasi Väisänen [c]

[a] *Top Analytica, Ruukinkatu 4, FI-20540 Turku, Finland*
[b] *Material Science and Environmental Engineering, Tampere University, FI-33101 Tampere, Finland*
[c] *SSAB Europe, Harvialantie 420, FI-13300 Hämeenlinna, Finland*

Received 14 October 2021; accepted 9 December 2021
Available online 13 December 2021

KEYWORDS

Zinc;
Hot dip galvanizing;
Supercritical CO_2;
Corrosion;
Carbonate

Abstract In a wet supercritical carbon dioxide atmosphere, carbon dioxide is dissolved into water and causes corrosion of zinc-coated steel. The first corrosion products appeared in singular nano-scale initiation sites, which gradually grew in number and size and ultimately covered the whole surface. Zinc hydroxy carbonate was detected as a rapidly forming needle-like corrosion product, which prevailed at short exposure times (from minutes to hours). A prolonged exposure caused conversion of zinc hydroxy carbonate to anhydrous zinc carbonate with high crystallinity and a stable, dense layer was formed on zinc. The chemical transition from zinc hydroxy carbonate to anhydrous carbonate was reported for the first time and is in the light of current literature unique for wet $scCO_2$ atmosphere.

1. Introduction

Zinc is commonly used to provide cathodic protection to steel (Zhang, 1996; Marder, 2000; Veleva et al., 2003). Hot dip galvanized steel construction elements are cost-efficient and can offer decades of prolonged corrosion resistance compared to bare steel. Corrosion phenomena of zinc-coated steels have been documented at least since 1837 (Morral, 1940), and today an abundant knowledge on zinc corrosion in various natural atmospheres, simulated environments, and accelerated laboratory exposures is available (Veleva et al., 2003; Morral, 1940; Anderson and Fuller, 1939; Falk et al., 1998; Diler et al., 2014; Yoo et al., 2014; Lindström and Odnevall Wallinder, 2011; Lindström et al., 2000; Prestat et al., 2017; Ohtsuka and Matsuda, 2003; Thomas et al., 2012; Kaesche, 1964). Recently, increased environmental concerns and global warming have initiated engineering efforts on sustainable technologies and regulation of CO_2 levels. CO_2 capture plants have been built and an interest to study metal corrosion in new artificial atmospheres has arisen (Choi et al., 2010; Cui et al., 2019). Furthermore, there is increased interest in

* Corresponding author.
E-mail address: ville.saarimaa@topanalytica.com (V. Saarimaa).
Peer review under responsibility of King Saud University.

Production and hosting by Elsevier

https://doi.org/10.1016/j.arabjc.2021.103636
1878-5352

environmentally sustainable technologies to protect metal from corrosion (Milošev and Frankel, 2018).

In natural outdoor environments, corrosion or patination of zinc is a long-term process that involves multiple dry and wet periods, various temperatures and interference of air impurities or trace element level gases. At first, humidity induces white rust formation, i.e. development of simple zinc oxides and hydroxides (Anderson and Fuller, 1939; Maeda, 1996). Even at very low carbon dioxide levels, the natural patination process bonds carbonate ions to the simple zinc oxides and hydroxides, and results in precipitation of more complex zinc hydroxy carbonates. Although exact chemical composition of these carbonates can vary, and several subgroups of precipitates are commonly found in environments containing SO_2 and NaCl, within a couple of years these complex, stable precipitates have mostly suppressed the electrochemical activity that occurs on bare, unprotected zinc surfaces (Mor and Beccaria, 1975).

Artificial supercritical carbon dioxide ($scCO_2$) environments contain significantly higher carbon dioxide concentrations than natural environments. A pure $scCO_2$ atmosphere is not detrimental to any metals, but even small amounts of impurities or water in a $scCO_2$ system are sufficient to initiate aggressive corrosion (Choi et al., 2010; Falk et al., 1998). The corrosion of steel pipeline systems of CO_2 capture plants is well documented and an ongoing research theme (Cui et al., 2019; Halseid et al., 2014; Dugstad et al., 2010; Dugstad and Halseid, 2012). However, the corrosion of galvanized steel in wet $scCO_2$ systems is not yet thoroughly studied.

The reaction steps that have been suggested to occur for zinc-coated steel in wet $scCO_2$ systems are composed of following reactions. Zinc corrosion is initiated by electrochemical activity on the surface: anodic zinc dissolution is balanced with cathodic oxygen reduction and hydrogen evolution reactions (Zhang, 1996). Hydrogen evolution is prominent and increases as a function of CO_2 dissolution into water (Kaleva et al., 2020). Dissolved Zn^{2+} ions are combined with hydroxyl groups, which may cause partial precipitation (Kaleva et al., 2020; Zaraska et al., 2017; Bockelmann et al., 2017; Mokaddem et al., 2010; Rayner-Canham, 2000). CO_2 dissolution into water also leads to the presence of carbonate ions (CO_3^{2-} and HCO_3^-) in the aqueous medium (Davis and Oliver, 1972). These ions are readily attracted to the zinc hydroxy complexes and as a result, zinc carbonates start to precipitate on the surface (Zaraska et al., 2017; Kannangara and Conway, 1987; Gaur et al., 2010; Bozbaş and Erkey, 2015). It has also been suggested that in addition to direct reactions with Zn^{2+} and OH^- ions, simple zinc oxide can be a reaction intermediate prior to carbonate formation (Kaleva et al., 2020).

In previous investigations, wet $scCO_2$ atmosphere has been thoroughly studied as a reactive medium for zinc-coated steel with in-situ and ex-situ experiments (Kaleva et al., 2020; Saarimaa et al., 2018; Kaleva et al., 2017). These previous studies report zinc hydroxy carbonate and zinc carbonate as the primary zinc corrosion products in wet $scCO_2$. The reaction parameters chosen for the current study were chosen based on the previous studies. The main aim of this study was to shed light on the reaction kinetics of corrosion product formation. However, an abrupt, exposure time-dependent change in chemical composition of the formed corrosion products was observed, and the main focus was shifted to detailed analytical determinations and discussions around the chemical transition that has not previously been reported.

2. Materials and methods

2.1. Material and pretreatment

Hot dip galvanized steel was obtained from SSAB Europe. The zinc bath contained about 0.2 wt-% Al, and the final zinc coating weight was 275 g/m^2. The zinc sheet was cut to 10 × 15 cm pieces and the specimens were cleaned with a two-stage laboratory cleaning process using Gardoclean 338 (Chemetall) at a free alkalinity of 4–5 meq/L in both baths. The temperature was 55–60 °C, the holding time 4 s per bath and the panels were rinsed in subsequent two-stage water spray chambers, operating at the same temperature as the alkaline cleaning baths. Finally, the samples were dried in a furnace at 60 °C for 10 min.

2.2. Supercritical carbon dioxide exposure

The cleaned panels were exposed in a reactor (volume 1.57 L, width 106 mm, height 268 mm, material: 316L grade stainless steel) that was pressurized with CO_2 gas. The reactor temperature was 40 °C and the pressure was 100 bar. 30 mL of deionized water was put into the reactor with the specimen at the start of each exposure to create a corrosive wet $scCO_2$ atmosphere. The amount of water was higher than the CO_2 dissolving capacity. There was no initial physical contact between the water and the panel in the reactor. Parallel samples were prepared. The exposure times were: 0 min (unexposed reference), 5 min, 10 min, 30 min, 1 h, 2 h, 3 h, 4 h, 8 h, 16 h and 1 week.

2.3. Quantification of corrosion products

The corrosion products were quantified by glycine extraction and XRF measurement according to a previously developed procedure (Saarimaa et al., 2018). The quantification was performed with an XRF (Epsilon 3XL, PANalytical) using a 50 kV voltage, a 109 μA current, a 180 s measurement time, and an Ag filter.

2.4. Surface analyses

SEM imaging was carried out with a ZEISS Gemini 450 field emission scanning electron microscope. A Bruker QUANTAX FlatQUAD EDS system was employed for element analysis at 3 kV acceleration voltage. A Bruker eFLASH FS electron backscatter diffraction detector (EBSD) was employed for zinc crystal orientation determination. EBSD was run at 20 kV and 5nA, with a 160x120 EBSP resolution and 15 ms exposure time. Cross sections for SEM imaging were prepared by broad ion beam milling (Ilion + Advantage Precision, Model 693, Gatan Inc) using a 6 kV voltage. FTIR measurements were done with a Spectrum two spectrometer equipped with single reflection diamond (Perkin Elmer). Raman measurements were carried out with a Renishaw InVia Qontor confocal Raman microscope with a 532 nm laser paired with an 1800 L/mm grating.

3. Results

3.1. SEM images of exposed samples

An unexposed hot dip galvanized steel surface had a mostly flat appearance with some skin passing-induced roughness (Fig. 1). The zinc surface became partially covered by patina already at very short (5–30 min) exposure times (Fig. 1). Corrosion product formation was initiated from multiple singular sites featuring nano-scale rods (Fig. 2). Similar initial nanostructures have been reported to form during zinc anodization (Zaraska et al., 2017). The initial nano-rods grew in size and showed a needle-like appearance until 2-hour exposure (Fig. 1, Fig. 3). The surface coverage of the corrosion products increased as a function of exposure time, indicating that the nano-scale growth initiation sites gradually developed macroscopic corrosion products. The length of the needles was greatest at the 2-hour exposure, which indicates that the length of the needles increases by a dynamic, stepwise whisker growth mechanism once the corrosion has been initiated on the reactive sites of the surface (Fig. 1, Fig. 3) (Zaraska et al., 2017; Saarimaa et al., 2018; Pillai and Ittyachen, 1978; Wang et al., 2011; Gong et al., 2017). In other words, the corrosion mechanism transitions quickly from corrosion initiation site formation to growth of the already-formed corrosion products.

The needle-like corrosion products prevailed up to 2-hour exposure, after which the needles disappeared (Fig. 1, Fig. 3). Cross section imaging shows how the porous surface layer is with time replaced with a dense patina layer (Fig. 3). A compact layer of corrosion products is less permeable to metal dissolution and slows down further dissolution and precipitation both physically and chemically (Mor and Beccaria, 1975; Saarimaa et al., 2018; Liang et al., 2013; Zhang et al., 2016). Close-up SEM images revealed the smooth surface of the protruding needles at short exposure time (Fig. 4, left). Above 2-hour exposure the shape of the needles was still visible in low magnification images, but they were now aligned in the plane of the zinc surface and not protruding from the surface (Fig. 4, right). Furthermore, the fine structure of the needles was disturbed. Instead of straight and narrow orientation they became distorted, and their fine structure was built up of fragmented layers. The residual transformed needles were visible on the surface at 4 h – 16 h exposures but could not be distinguished at 1 week exposure (Fig. 1). This is presumably because of extended patina layer thickness growth that covered the initial corrosion products.

3.2. Molecular spectroscopy of exposed samples (FTIR and Raman)

Raman spectra were recorded on $scCO_2$-exposed specimens at different exposure times. The CO_3^{2-} symmetric vibration (v_1) is the most prominent Raman stretching signal for zinc carbonate corrosion products. It is clearly seen that the center of the vibration is shifted to slightly lower wavelength when going from 2 to 4-hour exposure time (Fig. 5). It has been reported in previous reports that the shift is related to presence of hydroxyl groups (Saarimaa et al., 2018). The symmetric stretching vibration for both anhydrous and hydrous zinc carbonate is centered at 1090–1100 cm^{-1}, the anhydrous form close to the low end and the hydrous form close to the high end of the range (Adler and Kerr, 1963; Burgio and Clark, 2001; Carbucicchio et al., 2008). The result are in line with earlier

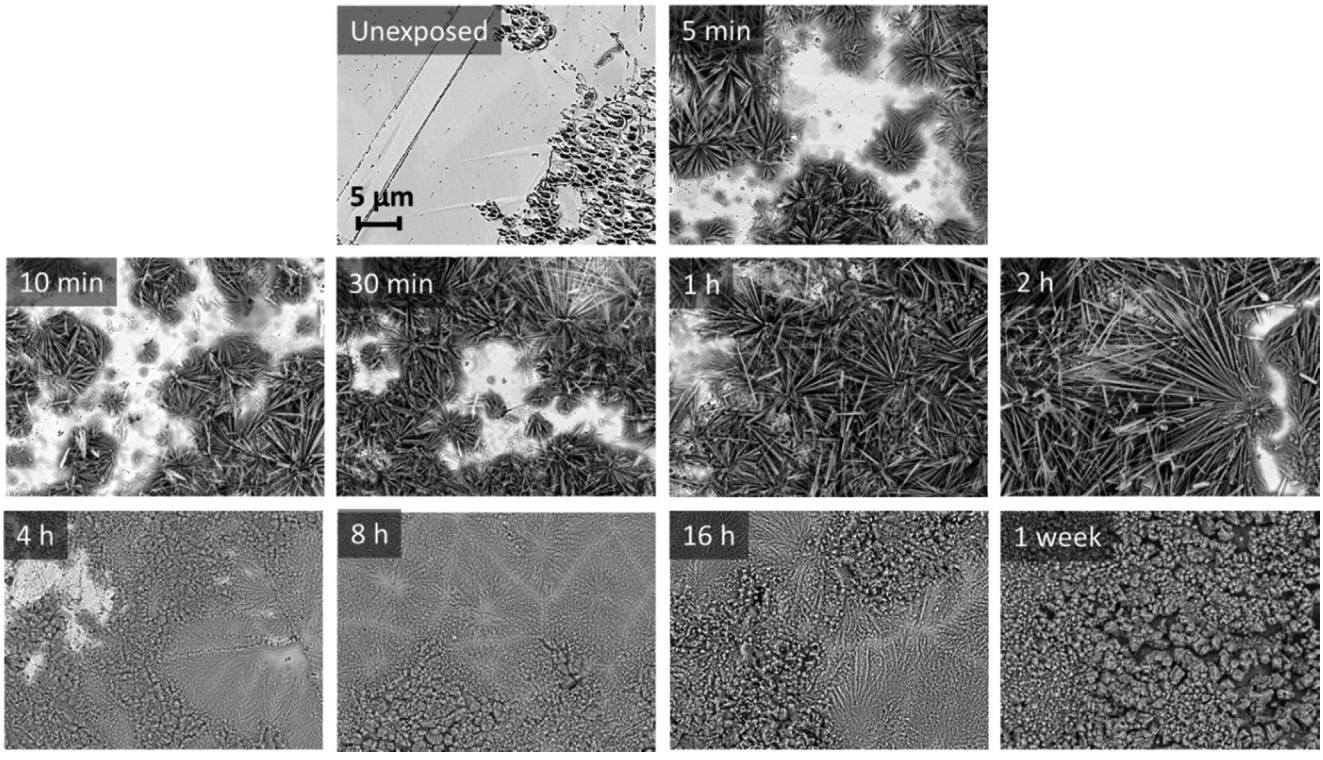

Fig. 1 Backscattering electron images (at 10 kV accelerating voltage) of exposed samples (top view).

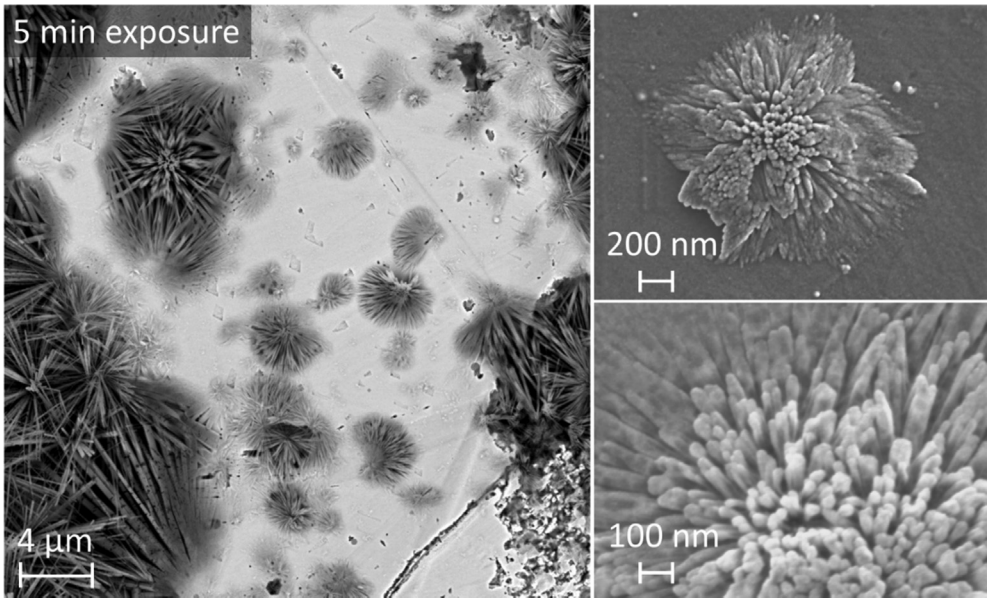

Fig. 2 Backscattering electron image (at 10 kV accelerating voltage) of corrosion initiation sites on 5 min exposed galvanized panel (left) and close-up secondary electron images (at 1 kV accelerating voltage) of a nano-scale initiation site (right).

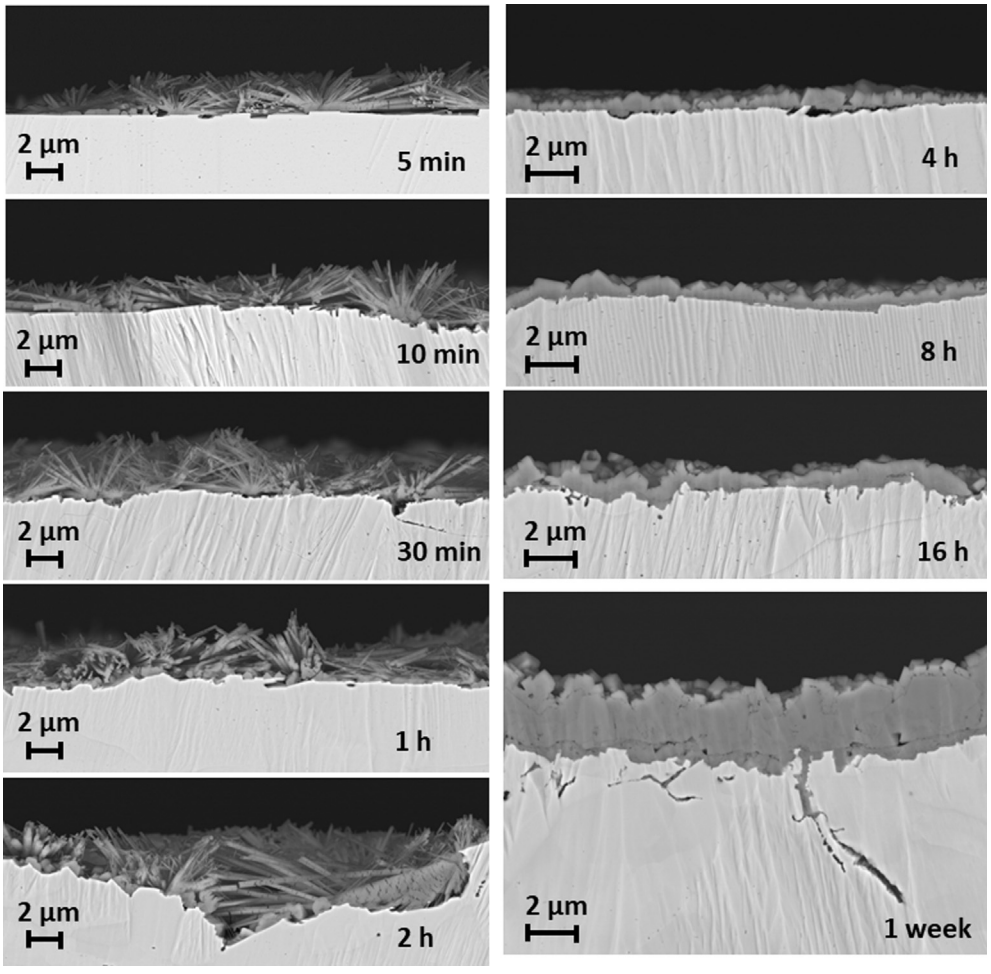

Fig. 3 Backscattering electron images (at 10 kV accelerating voltage) of cross sections from exposed samples.

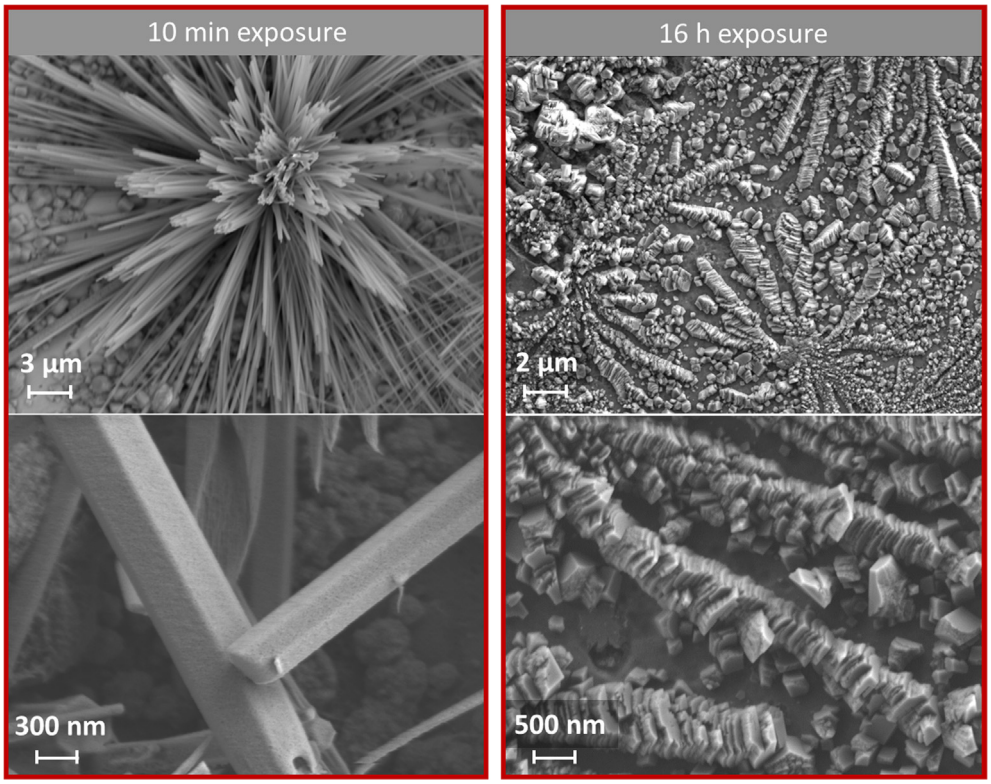

Fig. 4 Secondary electron images (at 10 kV accelerating voltage) of exposed specimens before (10 min) and after (16 h) transition of surface morphology.

investigations with similar structures (Kaleva et al., 2020; Saarimaa et al., 2018).

The data was further processed to produce v_1 vibration peak widths (Fig. 6). The hydroxyl group containing carbonate (short exposure time) has broader peaks than the anhydrous form (long exposure time). The peak width is associated with material crystallinity. A single crystal appears as a symmetric and narrow peak. Asymmetry and tailing of Raman peaks indicate that a sample contains a mixture of various crystal sizes. Zinc hydroxy carbonate is suggested to be a mixed phase compound, while the anhydrous carbonate has a single phase final crystal structure (Saarimaa et al., 2018; Miles et al., 2015). Thus, the crystallinity of the wet $scCO_2$ induced zinc corrosion products is significantly increased by a prolonged exposure and conversion to anhydrous patina.

FTIR spectroscopy confirmed the chemical transition (Fig. 7). The strongest FTIR mode related to the CO_3^{2-} group is the v_3 antisymmetric stretching, which for zinc hydroxy carbonate is manifested by two absorbance modes at 1383 and at 1520 cm-1 (Frost et al., 2008; Hales and Frost, 2007). These modes were clearly seen at exposures until 2 h. Furthermore, OH^- stretching modes were present as a broad peak at 3000–3500 cm-1 (Ghose, 1964; Loring et al., 2011). The two v_3 antisymmetric stretching modes changed to one mode at 1390 cm^{-1}, and the OH^- stretching modes disappeared after 2-hour exposure, which confirms transition to anhydrous zinc carbonate (Frost et al., 2008). Fast preparation of nanocrystalline hydrozincite in water-CO_2 phase has been reported earlier, which supports the findings in this study (Turianicová et al., 2016). A zinc hydroxy carbonate named hydrozincite, $Zn_5(CO_3)_2(OH)_6$ is probably the most common complex zinc corrosion product formed in unpolluted environments (Almeida et al., 2000). Anhydrous zinc carbonate is rarely

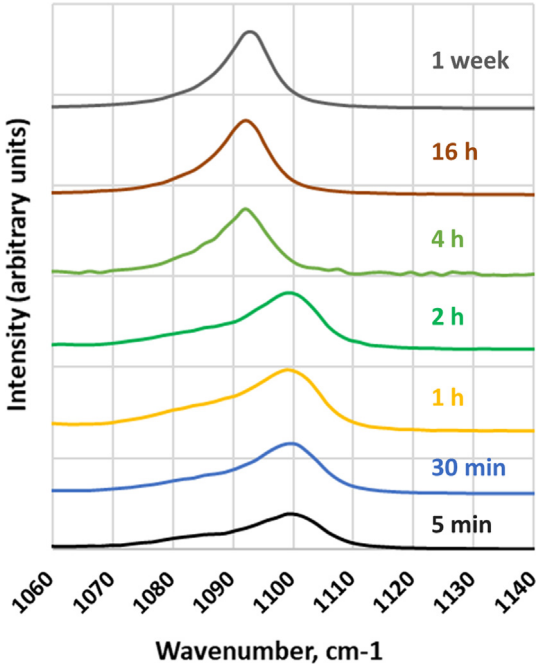

Fig. 5 Raman spectra of the CO_3^{2-} symmetric stretching vibration mode (v_1) at different exposure times.

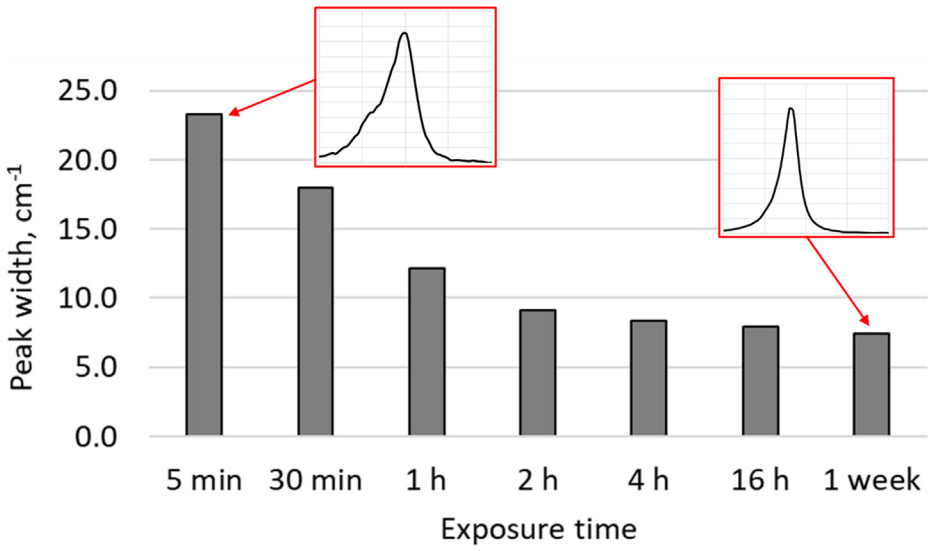

Fig. 6 Peak width of CO_3^{2-} symmetric stretching vibration of corroded samples at different exposure times.

found in outdoor exposed or laboratory exposed zinc sheets, which makes it a unique end product in wet $scCO_2$ exposure (Alwan and Williams, 1979).

3.3. Extraction and quantification of zinc corrosion products

A summary of selective extraction and quantification data of zinc ions bonded to hydroxy carbonate and to anhydrous carbonate is shown in Fig. 8. An unexposed sample had very little oxidized zinc on the surface. Wet $scCO_2$ exposure caused a rapid increase in the concentration of corroded zinc, zinc hydroxy carbonate being the main corrosion product at short exposure times. The growth of zinc hydroxy carbonate layer was systematic up to 2-hour exposure. After that, the dominating corrosion product was anhydrous zinc carbonate. Individual exposures were independent from other exposures, which means that a certain sample was kept under exposure the whole specific exposure time without removal or addition of other samples in the reactor. This confirms that the zinc hydroxy carbonate was converted to anhydrous zinc carbonate after the 2-hour exposure time. During the transition (2 h → 4 h), the total amount of Zn^{2+} in the corrosion products remained on a same level and further increase was obtained only after a greatly increased exposure time (16 h → 1 week). The continuous increase in the amount of early, hydroxyl group containing corrosion products was disrupted once the anhydrous zinc carbonate started to dominate. This indicates that the growth rate for the hydroxy carbonate is much faster than the growth rate of anhydrous carbonate.

3.4. Discussion on transition mechanism

Zinc hydroxy carbonates are stable at low temperature and CO_2 pressure, as indicated by their great abundancy on zinc exposed to natural atmospheres or artificial atmospheres with low to moderate CO_2 partial pressure (Jambor, 1964; Vágvölgyi et al., 2008), but clearly in a supercritical system with sufficient exposure time the anhydrous zinc carbonate is the prevailing form. The hydroxyl groups in zinc hydroxy carbonates are bonded as structural OH groups and as crystallization water. Mineralization studies in the literature have shown that some hydroxyl group-containing minerals are metastable and ready to exchange their OH groups for carbonate groups when a necessary energy barrier is exceed (Loring et al., 2012). Based on the results of this study the supercritical conditions together with a mild temperature drive the dehydration process of the initial hydroxyl group containing corrosion products to an end within a few of hours. Anhydrous carbonate has been reported to form also on simple steel elements (without galvanizing) (Carbucicchio et al., 2008; Hua et al., 2015).

Thermal decomposition of various hydroxy carbonates is a well-known phenomenon (Vágvölgyi et al., 2008; Wahab et al., 2008; Kolodziejczak-Radzimska and Jesionowski, 2014; Kaleva et al., 2018; Joshi et al., 2019; Hartman et al., 2001).

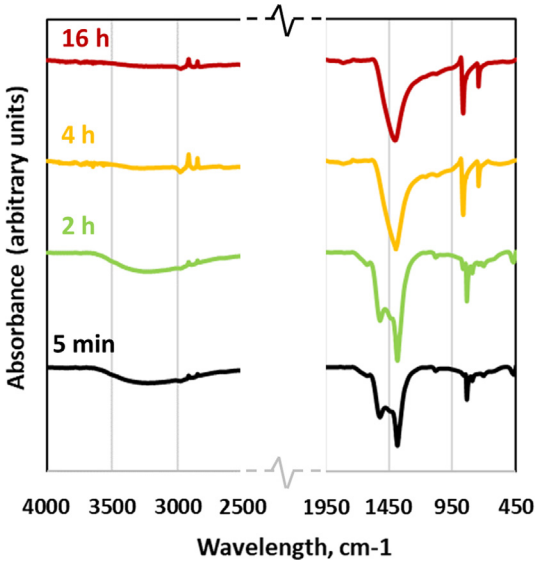

Fig. 7 FTIR spectra of exposed samples before and after chemical transition from OH^- group containing carbonate to anhydrous carbonate.

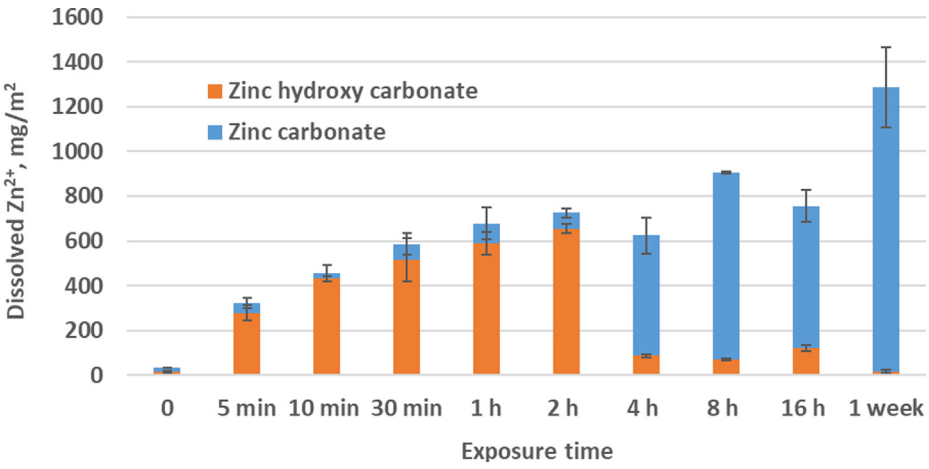

Fig. 8 The amount of oxidized zinc bonded to zinc corrosion products at different exposure times.

Dehydration (removal of non-structural water by heating) of zinc hydroxy carbonate can take place even at low temperature (38 °C), but further removal of structural water requires an energy sufficient to reorganize the hydrogen bonds and is normally not achieved without simultaneous removal of CO_2 (Vágvölgyi et al., 2008; Ihli et al., 2014). The decomposition of zinc hydroxy carbonate typically requires an initiation temperature greater than 150 °C (Kanari et al., 2004) and is terminated at much higher temperatures (~250–600 °C) (Vágvölgyi et al., 2008). Decomposition can also take place at a lower temperature in the presence of a chemical mediator but a substantially longer reaction time is then required (Joshi et al., 2019). Apart from removal of adsorbed (non-structural) water from zinc hydroxy carbonate, decomposition takes place as a single-step transition to zinc oxide, and no intermediates have been reported (Vágvölgyi et al., 2008; Joshi et al., 2019). The formation of zinc hydroxy carbonate and anhydrous zinc carbonate has been shown to depend on the partial pressure of CO_2 (Vágvölgyi et al., 2008), the latter being more prominent at elevated partial pressures, but this finding cannot explain why zinc hydroxy carbonate was first formed in wet $scCO_2$ atmosphere and later converted to $ZnCO_3$ (the pressure being stable). In another study, dehydration and crystallization of amorphous calcium carbonate has been proposed to occur via a dissolution-reprecipitation mechanism, where the structural water lowers the energy barrier and functions as a mediator (Ihli et al., 2014). The crystal lattices of a metastable phase were destroyed by the structure conversion process (Ihli et al., 2014), which provides a plausible explanation for the degradation of the needle-like corrosion products in this study (Fig. 4).

Based on the existing literature, the observed transition of zinc hydroxy carbonate to zinc carbonate has not been reported earlier and may be exclusive to supercritical carbon dioxide atmosphere. It should be noted that transition of amorphous intermediates to crystalline compounds are not fully understood (Ihli et al., 2014), and clarification of the exact transition mechanism reported in this study requires more investigation.

3.5. Observations on corrosion product formation

Wet $scCO_2$ is a very corrosive environment to zinc, as shown by the exposures. The main corrosion initiation reactions in such atmospheres have been reported to be: (i) zinc dissolution (anodic reaction) and (ii) hydrogen evolution, oxygen dissolution (cathodic reactions) and carbon dioxide dissolution (results in formation of carbonic acid) (Kaleva et al., 2020). In Fig. 9, zinc dissolution sites can be seen as hexagonal cavities on the metal surface. Such hexagonal forms have been observed earlier when zinc corrosion products have been extracted from a zinc surface (Zhang, 1996; Saarimaa et al., 2018). Remarkably, the zinc carbonate deposits in Fig. 9, that is the carbon and oxygen-rich sites in the element map, do not cover all the zinc dissolution sites. This indicates presence of a thin aqueous layer on the metal surface during the dissolution and precipitation process. The importance of an aqueous surface film on zinc carbonate formation has been highlighted in the literature (McGrail et al., 2009; M. O'Connor, 30b (1975)). This reaction medium allows mobility of ions (Zn^{2+}, OH^-, CO_3^{2-}, HCO_3^-) (Kaleva et al., 2020), and precipitation of corrosion products at the sites nearby zinc dissolution sites is possible. The presence of the reaction medium is also indicated by the relatively even thickness of the corrosion product layers independent on the exposure time (Fig. 3). The increase in the length of the needle-like corrosion products proceeds close to the surface, where the ions participating in the growth are available.

Zinc crystal orientation is defined during zinc solidification and skin passing processes at the end of the hot dip galvanizing process (Marder, 2000; Leidheiser and Kim, 1978). Zinc crystals may grow in basal planes parallel to surface or perpendicular to surface, and also in orientations between these extremes (Kim et al., 2019; Chilton et al., 1969). Individual zinc grains grow in one crystallographic growth direction. Zinc dissolution pattern reveals the crystal orientation. In Fig. 10, examples of various zinc dissolution patterns are shown. The cross-section images in Fig. 10 show sites with zinc crystal orientation parallel to the surface (a and b) and sites with crystal orientation perpendicular to the surface (c) and sites with a tilted crystal orientation (d). The crystallographic zinc orientations were measured by EBSD and the simplified orientations are shown in the lower left corners of the images (Fig. 10). Based on these results the corrosion product growth in wet $scCO_2$ take place on all grains independent on the local zinc crystal orientation. However, in the literature the crystal orientation has been stated to affect the local grain reactivity

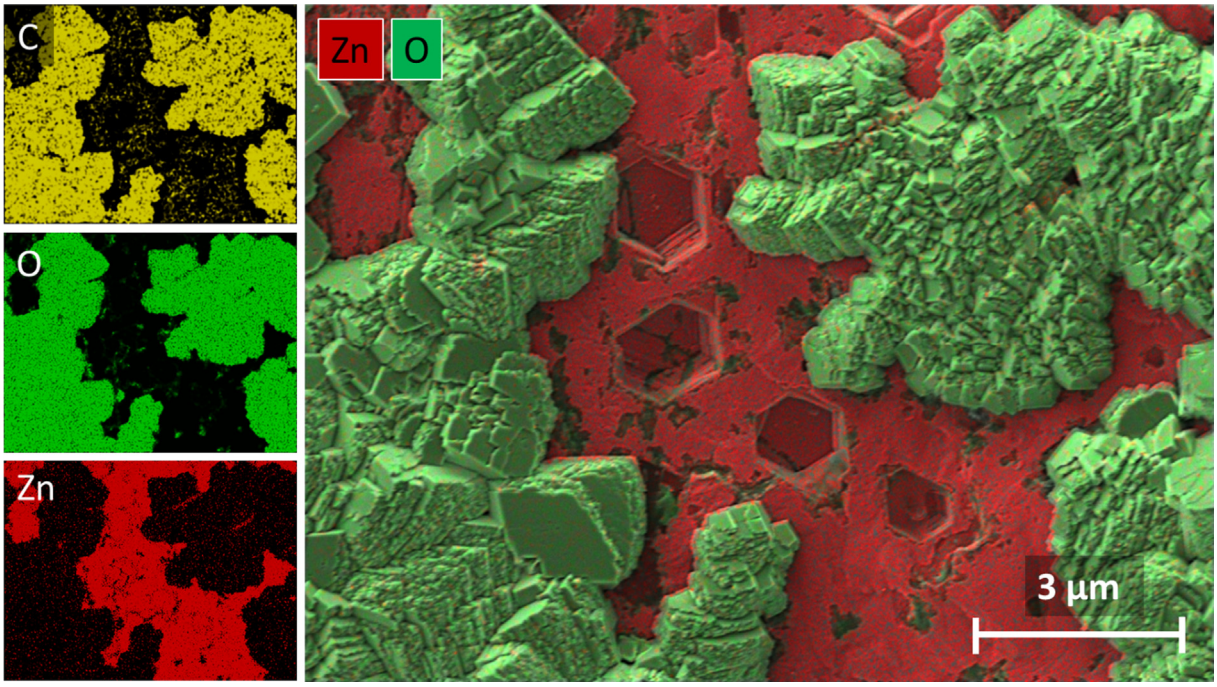

Fig. 9 SEM EDS element maps (at 3 kV accelerating voltage) of an exposed sample after 4-hour exposure.

(Kim and Leidheiser, 1978; Mataigne et al., 2007; Gentile et al., 2010; Ruff, 1974).

In Fig. 11. the arrow "1″ points to a zinc dissolution pattern where the original zinc crystals have oriented perpendicular to the surface, while the arrow "2" points to a dissolution site on the adjacent zinc grain with crystal orientation parallel to the surface. In the literature the planes parallel to the surface have been indicated to be less reactive than the planes perpendicular to the surface (Mataigne et al., 2007; Gentile et al., 2010; Ruff, 1974), which is also seen in Fig. 10 when comparing the vol-

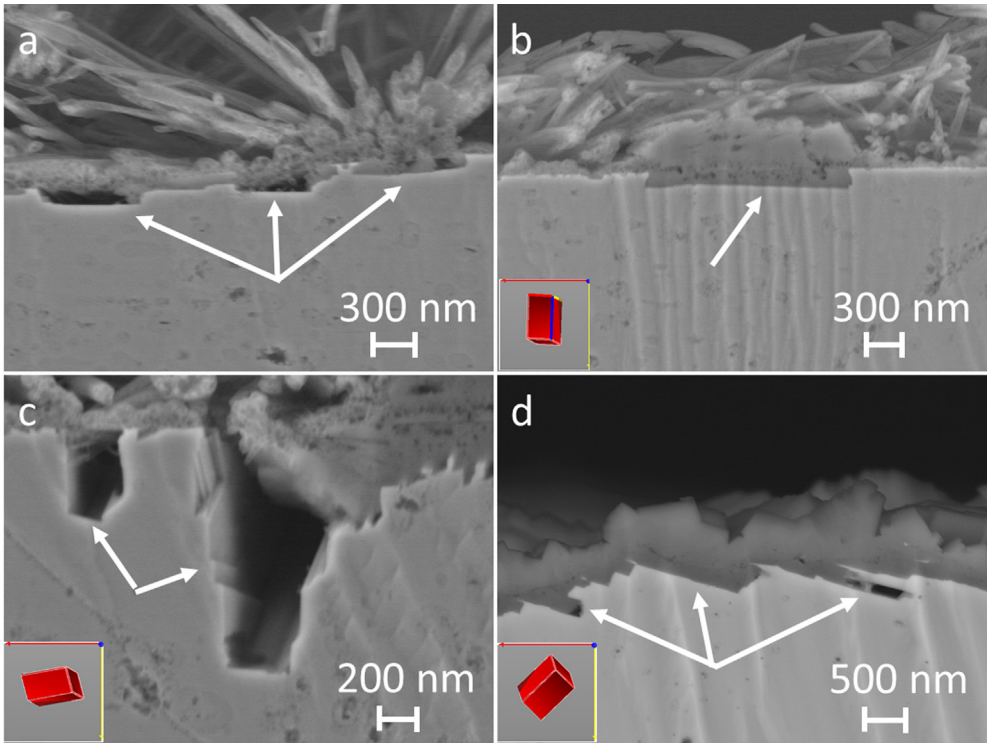

Fig. 10 Backscattering electron images (at 10 kV accelerating voltage) of exposed samples showing various zinc dissolving patterns. Simplified zinc crystal orientations, measured by EBSD, are shown in lower left corners of the images.

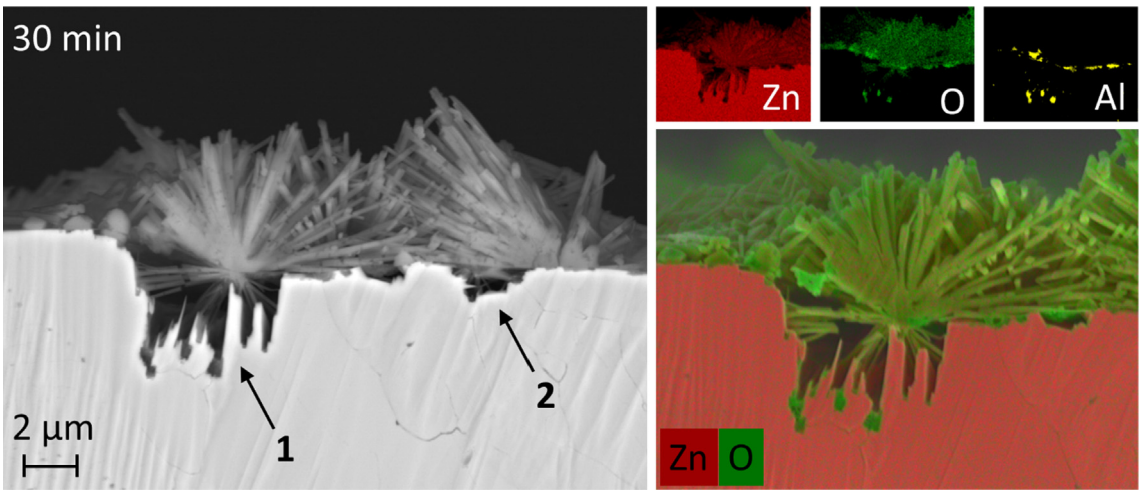

Fig. 11 Backscattering electron image (left, recorded at 10 kV accelerating voltage) and EDS element maps (at 3 kV accelerating voltage) of a corroded site after 30 min exposure.

ume of the dissolved zinc voids in adjacent grains ("1" showing a site with perpendicular and "2" showing a site with parallel zinc crystal orientation). This topic, however, requires more investigation. It can be further seen that the needles (oxygen and zinc containing corrosion products) grow from a singular initiation point to all directions, even deeper into the zinc coating into the void where zinc dissolution has taken place, ultimately filling the void (Saarimaa et al., 2021). The hot dip galvanized zinc coating contains inherently some aluminum precipitates, which are seen as individual islands on the surface and within the coating. The dissolution of the perpendicularly grown zinc crystals has stopped at the aluminum inclusions (Fig. 11) (Saarimaa et al., 2020).

4. Conclusions

Wet supercritical CO_2 is a very corrosive atmosphere to zinc, and nano-scale corrosion initiation sites start to grow instantly when a zinc surface is exposed to it. Zinc is dissolved and subsequently precipitated as two main carbonates on hot dip galvanized steel: rapidly forming zinc hydroxy carbonate and slowly forming anhydrous zinc carbonate. Hexagonal dissolving patterns on zinc surface adjacent to carbonate precipitates indicate that a thin aqueous film is present on the metal surface and enables mobility of the anion and cations during the reaction. Zinc dissolution is a dynamic process and facilitates with time growth of initial nano-scale corrosion products to macroscopic crystalline materials. During the first minutes and hours, the amount of zinc hydroxy carbonate grows steadily. The physical appearance of the corrosion products abruptly changed after prolonged exposure to a denser layer without protruding needles. Electron microscopy and molecular spectroscopy confirmed that the zinc hydroxy carbonate is a metastable form that under prolonged supercritical exposure releases its hydroxyl groups and converts to anhydrous zinc carbonate. Ultimately, a dense, stable carbonate layer with even surface coverage is formed. This anhydrous carbonate layer is not formed in natural atmosphere and can suppress the electrochemical activity of the underlying metallic zinc coating.

Declaration of Competing Interest

The authors declare that they have no known competing financial interests or personal relationships that could have appeared to influence the work reported in this paper.

References

Adler, H., Kerr, P., 1963. Infrared absorption frequency trends for anhydrous normal carbonates. Am. Miner. 48, 124–137.

Almeida, E., Morcillo, M., Rosales, B., 2000. Atmospheric corrosion of zinc. Part 1: rural and urban atmospheres. Br. Corros. J. 35, 284–288.

Alwan, A.K., Williams, P.A., 1979. Mineral formation from aqueous solution. Part I. The deposition of hydrozincite, Zn5(OH)6(CO3)2, from natural waters. Transit. Met. Chem. 4, 128–132. https://doi.org/10.1007/BF00618840.

Anderson, E.A., Fuller, M.L., 1939. Corrosion of zinc. Met. Alloy. 10, 282–287.

Bockelmann, M., Reining, L., Kunz, U., Turek, T., 2017. Electrochemical characterization and mathematical modeling of zinc passivation in alkaline solutions: A review. Electrochim. Acta. 237, 276–298. https://doi.org/10.1016/j.electacta.2017.03.143.

Bozbaş, S.E., Erkey, C., 2015. Supercritical deposition: Current status and perspectives for the preparation of supported metal nanostructures. J. Supercrit. Fluids. 96, 298–312. https://doi.org/10.1016/j.supflu.2014.09.036.

L. Burgio, R.J.H. Clark, *Library of FT-Raman spectra of pigments, minerals, pigment media and varnishes, and supplement to existing library of Raman spectra of pigments with visible excitation*, 2001. https://doi.org/10.1016/S1386-1425(00)00495-9.

Carbucicchio, M., Ciprian, R., Ospitali, F., Palombarini, G., 2008. Morphology and phase composition of corrosion products formed at the zinc-iron interface of a galvanized steel. Corros. Sci. 50, 2605–2613. https://doi.org/10.1016/j.corsci.2008.06.007.

Chilton, A.C., Stobo, J.J., Graham, M.R., Crocker, A.G., 1969. Grain growth in sheet zinc, Czechoslov. J. Phys. B. 19, 103–108.

Choi, Y.S., Nesic, S., Young, D., 2010. Effect of impurities on the corrosion behavior of CO2 transmission pipeline steel in supercritical CO2-water environments. Environ. Sci. Technol. 44, 9233–9238. https://doi.org/10.1021/es102578c.

Cui, G., Yang, Z., Liu, J., Li, Z., 2019. A comprehensive review of metal corrosion in a supercritical CO2 environment. Int. J. Greenh. Gas Control. 90, 1–17. https://doi.org/10.1016/j.ijggc.2019.102814.

Davis, A., Oliver, B., 1972. A vibrational-spectroscopic study of the species present in the CO2-H2O system. J. Solut. Chem. 1, 329–339.
Diler, E., Lescop, B., Rioual, S., Nguyen Vien, G., Thierry, D., Rouvellou, B., 2014. Initial formation of corrosion products on pure zinc and MgZn2 examinated by XPS. Corros. Sci. 79, 83–88. https://doi.org/10.1016/j.corsci.2013.10.029.
A. Dugstad, M. Halseid, Internal corrosion in dense phase CO2 transport pipelines - state of the art and the need for further R&D, in: NACE Int. Corros. Conf. 2012, NACE Corrosion, Texas, 2012: pp. 1–14.
Dugstad, A., Morland, B., Clausen, S., 2010. Corrosion of transport pipelines for CO2 - effect of water ingress. Energy Procedia2. 4, 3063–3070.
Falk, T., Svensson, J., Johansson, L., 1998. The role of carbon dioxide in the atmospheric corrosion of zinc. J. Electrochem. Soc. 145, 39–44.
Falk, T., Svensson, J., Johansson, L., 1998. The influence of CO2 and NaCl on the atmospheric corrosion of zinc, a laboratory study. J. Electrochem. Soc. 1 (145), 2993–2999.
Frost, R.L., Martens, W.N., Wain, D.L., Hales, M.C., 2008. Infrared and infrared emission spectroscopy of the zinc carbonate mineral smithsonite. Spectrochim. Acta - Part A Mol. Biomol. Spectrosc. 70, 1120–1126. https://doi.org/10.1016/j.saa.2007.10.027.
Gaur, A., Park, J.W., Jang, J.H., 2010. Metal-carbonate formation from ammonia solution by addition of metal salts - An effective method for CO2capture from landfill gas (LFG). Fuel Process. Technol. 91, 1500–1504. https://doi.org/10.1016/j.fuproc.2010.05.027.
Gentile, M., Koroleva, E.V., Skeldon, P., Noakes, T.C.Q., 2010. Influence of grain orientation on zinc enrichment and surface morphology of an Al-Zn alloy. Surf. Interface Anal. 42, 287–292.
Ghose, S., 1964. The crystal structure of hydrozincite. Acta Cryst. 17, 1051–1057.
Gong, B., Shi, T., Liao, G., Li, X., Huang, J., Zhou, T., Tang, Z., 2017. UV irradiation assisted growth of ZnO nanowires on optical fiber surface. Appl. Surf. Sci. 406, 294–300. https://doi.org/10.1016/j.apsusc.2017.02.153.
Hales, M.C., Frost, R.L., 2007. Synthesis and vibrational spectroscopic characterisation of synthetic hydrozincite and smithsonite. Polyhedron. 26, 4955–4962. https://doi.org/10.1016/j.poly.2007.07.002.
Halseid, M., Dugstad, A., Morland, B., 2014. Corrosion and bulk phase reactions in CO2 transport pipelines with impurities: Review of recent published studies. Energy Procedia. 63, 2557–2569. https://doi.org/10.1016/j.egypro.2014.11.278.
Hartman, M., Trnka, O., Veselý, V., Svoboda, K., 2001. Thermal dehydration of the sodium carbonate hydrates. Chem. Eng. Commun. 185, 1–16. https://doi.org/10.1080/00986440108912851.
Hua, Y., Barker, R., Charpentier, T., Ward, M., Neville, A., 2015. Relating iron carbonate morphology to corrosion characteristics for water-saturated supercritical CO2 systems. J. Supercrit. Fluids. 98, 183–193. https://doi.org/10.1016/j.supflu.2014.12.009.
Ihli, J., Wong, W.C., Noel, E.H., Kim, Y.Y., Kulak, A.N., Christenson, H.K., Duer, M.J., Meldrum, F.C., 2014. Dehydration and crystallization of amorphous calcium carbonate in solution and in air. Nat. Commun. 5, 1–10. https://doi.org/10.1038/ncomms4169.
Jambor, J.L., 1964. Studies of Basic Copper and Zinc Carbonates: 1-Synthetic Zinc Carbonates and Their Relationship ot Hydrozincite. Can. Mineral. 8, 92–108.
Joshi, S., Jones, L.A., Sabri, Y.M., Bhargava, S.K., Sunkara, M.V., Ippolito, S.J., 2019. Facile conversion of zinc hydroxide carbonate to CaO-ZnO for selective CO2 gas detection. J. Colloid Interface Sci. 558, 310–322. https://doi.org/10.1016/j.jcis.2019.09.103.
Kaesche, H., 1964. The passivity of zinc in aqueous solutions of sodium carbonate and sodium bicarbonate. Electrochim. Acta. 9, 338–394.
Kaleva, A., Saarimaa, V., Heinonen, S., Nikkanen, J.-P., Markkula, A., Väisänen, P., Levänen, E., 2017. Dissolution-Induced Nanowire Synthesis on Hot-Dip Galvanized Surface in Supercritical Carbon Dioxide. Nanomaterials. 7, 181–190. https://doi.org/10.3390/nano7070181.
Kaleva, A., Nikkanen, J., Heinonen, S., Saarimaa, V., Vuorinen, T., Levänen, E., 2018. Synthesis of ZnO nanowires with supercritical carbon dioxide and post heat treatment. Nanotechnology. 29, 1–7.
Kaleva, A., Tassaing, T., Saarimaa, V., Le Bourdon, G., Väisänen, P., Markkula, A., Levänen, E., 2020. Formation of corrosion products on zinc in wet supercritical and subcritical CO2: In-situ spectroscopic study. Corros. Sci. 174. https://doi.org/10.1016/j.corsci.2020.108850.
Kanari, N., Mishra, D., Gaballah, I., Dupré, B., 2004. Thermal decomposition of zinc carbonate hydroxide. Thermochim. Acta. 410, 93–100. https://doi.org/10.1016/S0040-6031(03)00396-4.
Kannangara, D.C.W., Conway, B.E., 1987. Zinc oxidation and redeposition processes in aqueous alkali and carbonate solutions. J. Electrochem. Soc. 134, 894–906.
Kim, S.G., Huh, J.Y., Chung, G.J., Hwang, H.S., Kim, S.H., 2019. Dendritic Morphologies of Hot-Dip Galvanized Zn-0.2 Wt Pct Al Coatings on Steel Sheets. Metall. Mater. Trans. A Phys. Metall. Mater. Sci. 50, 3186–3200. https://doi.org/10.1007/s11661-019-05263-4.
Kim, D.K., Leidheiser Jr., H., 1978. A chemical test for identifying the fraction of grains in the surface of galvanized steel that have orientations approximating (0001) - importance to paint adherence. Metall. Trans. B 1 (9B), 581–593.
Kolodziejczak-Radzimska, A., Jesionowski, T., 2014. Zinc oxide-from synthesis to application: A review. Materials (Basel). 7, 2833–2881. https://doi.org/10.3390/ma7042833.
Leidheiser, H., Kim, D.K., 1978. Paint adhesion following deformation as related to the surface structure of hot-dipped galvanized steel. SAE Tech. Pap., 749–754 https://doi.org/10.4271/780185.
Liang, J., Hu, Y., Wu, Y., Chen, H., 2013. Fabrication and corrosion resistance of superhydrophobic hydroxide zinc carbonate film on aluminum substrates. J. Nanomater. 2013. https://doi.org/10.1155/2013/139768.
Lindström, D., Odnevall Wallinder, I., 2011. Long-term use of galvanized steel in external applications. Aspects of patina formation, zinc runoff, barrier properties of surface treatments, and coatings and environmental fate. Environ. Monit. Assess. 173, 139–153. https://doi.org/10.1007/s10661-010-1377-8.
Lindström, R., Svensson, J.-E., Johansson, L.-G., 2000. The atmospheric corrosion of zinc in the presence of NaCl. The influence of carbon dioxide and temperature. J. Electrochem. Soc. 147, 1751–1757.
Loring, J., Thompson, C., Wang, Z., Joly, A., Sklarew, D., Schaef, H., Ilton, E., Rosso, K., Felmy, A., 2011. In situ infrared spectroscopic study of forsterite carbonation in wet supercritical CO2. Environ. Sci. Technol. 45, 6204–6210.
Loring, J., Thompson, C., Zhang, C., Wang, Z., Schaef, H., Rosso, K., 2012. In situ infrared spectroscopic study of brucite carbonation in dry to water-saturated supercritical carbon dioxide. J. Phys. Chem. A. 116, 4768–4777.
M. OConnor, A study of the kinetics of the basic zinc carbonate formation reaction, *Z. Naturforsch.* 30b (1975) 665–668
Maeda, S., 1996. Surface chemistry of galvanized steel sheets relevant to adhesion performance. Prog. Org. Coatings. 28, 227–238. https://doi.org/10.1016/0300-9440(95)00610-9.
Marder, A.R., 2000. The metallurgy of zinc-coated steel. Prog. Mater. Sci. 45, 191–271. https://doi.org/10.1016/S0079-6425(98)00006-1.
Mataigne, J.-M., Vaché, V., Repoux, M., 2007. Surface chemistry and reactivity of skin-passed hot dip galvanized steel. Rev. Métallurgie. 106, 41–47.
McGrail, B.P., Schaef, H.T., Glezakou, V.A., Dang, L.X., Owen, A. T., 2009. Water reactivity in the liquid and supercritical CO2 phase: Has half the story been neglected? Energy Procedia. 1, 3415–3419. https://doi.org/10.1016/j.egypro.2009.02.131.

Miles, D., Cameron, P., Mattia, D., 2015. Hierarchical 3D ZnO nanowire structures via fast anodization of zinc. J. Mater. Chem. A. 3, 17569–17577.

Milošev, I., Frankel, G.S., 2018. Review—Conversion Coatings Based on Zirconium and/or Titanium. J. Electrochem. Soc. 165, C127–C144. https://doi.org/10.1149/2.0371803jes.

Mokaddem, M., Volovitch, P., Ogle, K., 2010. The anodic dissolution of zinc and zinc alloys in alkaline solution. I. Oxide formation on electrogalvanized steel. Electrochim. Acta. 55, 7867–7875. https://doi.org/10.1016/j.electacta.2010.02.020.

Mor, E., Beccaria, A., 1975. Effect of temperature on the corrodibility of copper and zinc in synthetic sea water. Corrosion1. 31, 275–279.

F.R. Morral, X-ray analysis of corrosion products from galvanized sheets, in: *77th Gen. Meet.*, 1940: pp. 279–288.

Ohtsuka, T., Matsuda, M., 2003. In situ Raman spectroscopy for corrosion products of zinc in humidified atmosphere in the presence of sodium chloride precipitate. Corrosion. 59, 407–413.

Pillai, K., Ittyachen, M., 1978. Growth and kinetic studies of lead carbonate whiskers in silica gel. Pramana-J. Phys. 10, 613–619.

Prestat, M., Holzer, L., Lescop, B., Rioual, S., Zaubitzer, C., Diler, E., Thierry, D., 2017. Microstructure and spatial distribution of corrosion products anodically grown on zinc in chloride solutions. Electrochem. Commun. 81, 56–60. https://doi.org/10.1016/j.elecom.2017.06.004.

G. Rayner-Canham, Descriptive Inorganic Chemistry, in: Descr. Inorg. Chem., 2nd Editio, W.H. Freeman and Company, New York, 2000: p. 509. https://doi.org/10.1016/c2014-0-02460-4.

Ruff, A.Q., 1974. Grain orientation dependence of reactivity in polycrystalline titanium after anodic polarization. Metall. Mater. Trans. B. 5, 601–603.

Saarimaa, V., Kaleva, A., Paunikallio, T., Nikkanen, J.-P., Heinonen, S., Levänen, E., Väisänen, P., Markkula, A., 2018. Convenient extraction method for quantification of thin zinc patina layers. Surf. Interface Anal. 50. https://doi.org/10.1002/sia.6429.

Saarimaa, V., Kaleva, A., Nikkanen, J.-P., Manni, J., Lange, C., Paunikallio, T., Laihinen, T., Heinonen, S., Levänen, E., Väisänen, P., Markkula, A., 2018. Tailoring of Versatile Surface Morphologies on Hot Dip Galvanized Steel in Wet CO2: Aspects on Formation, Barrier Properties, and Utilization as a Substrate for Coatings. ACS Appl. Mater. Interfaces. 10, 21730–21739. https://doi.org/10.1021/acsami.8b05034.

Saarimaa, V., Fuertes, N., Persson, D., Zavalis, T., Kaleva, A., Nikkanen, J.-P., Levänen, E., Heydari, G., 2020. Assessment of pitting corrosion in bare and passivated (wet scCO2-induced patination and chemical passivation) hot-dip galvanized steel samples with SVET, FTIR, and SEM (EDS). Mater. Corros. https://doi.org/10.1002/maco.202011653.

Saarimaa, V., Kaleva, A., Levänen, E., Väisänen, P., Markkula, A., 2021. Aspects on Early-Stage Corrosion of Different Zinc Alloys: Wet scCO2-Induced Corrosion. Corrosion. 77, 16–28. https://doi.org/10.5006/3668.

Thomas, S., Birbilis, N., Venkatraman, M.S., Cole, I.S., 2012. Corrosion of zinc as a function of pH. Corrosion. 68, 1–9. https://doi.org/10.5006/1.3676630.

Turianicová, E., Kaňuchová, M., Zorkovská, A., Holub, M., Bujňáková, Z., Dutková, E., Baláž, M., Findoráková, L., Balintová, M., Obut, A., 2016. CO2utilization for fast preparation of nanocrystalline hydrozincite. J. CO2 Util. 16, 328–335. https://doi.org/10.1016/j.jcou.2016.08.007.

Vágvölgyi, V., Hales, M., Martens, W., Kristóf, J., Horváth, E., Frost, R.L., 2008. Dynamic and controlled rate thermal analysis of hydrozincite and smithsonite. J. Therm. Anal. Calorim. 92, 911–916. https://doi.org/10.1007/s10973-007-8846-5.

L. Veleva, R.D. Kane, Atmospheric corrosion, in: B.S. Covino Jr., S. D. Cramer (Eds.), ASTM Handb. Vol. 13A. Corros. Fundam. Test. Prot., *ASM International Materials Park, Ohio*, 2003: pp. 196–209.

Wahab, R., Ansari, S.G., Soon Kim, Y., Dar, M.A., Shin, H.-S., 2008. Synthesis and characterization of hydrozincite and its conversion into zinc oxide nanoparticles. J. Alloys Compd. 461, 66–71.

Wang, N., Chen, M., Ni, H.W., 2011. Preparation of magnesium carbonate whisker from magnesite tailings. IOP Conf. Ser. Mater. Sci. Eng. 18. https://doi.org/10.1088/1757-899X/18/22/222013.

Yoo, J.D., Ogle, K., Volovitch, P., 2014. The effect of synthetic zinc corrosion products on corrosion of electrogalvanized steel. II. Zinc reactivity and galvanic coupling zinc/steel in presence of zinc corrosion products. Corros. Sci. 83, 32–37. https://doi.org/10.1016/j.corsci.2013.12.024.

Zaraska, L., Mika, K., Syrek, K., Sulka, G.D., 2017. Formation of ZnO nanowires during anodic oxidation of zinc in bicarbonate electrolytes. J. Electroanal. Chem. 801, 511–520. https://doi.org/10.1016/j.jelechem.2017.08.035.

Zhang, X.G., 1996. Corrosion and Electrochemistry of Zinc. Springer Science + Business Media, LCC, New York.

Zhang, D., Wang, L., Qian, H., Li, X., 2016. Superhydrophobic surfaces for corrosion protection: a review of recent progresses and future directions. J. Coatings Technol. Res. 13, 11–29. https://doi.org/10.1007/s11998-015-9744-6.